Intravascular laser speckle imaging catheter for the mechanical evaluation of the arterial wall

Zeinab Hajjarian,[a] Jingqun Xi,[a] Farouc A. Jaffer,[b] Guillermo J. Tearney,[a] and Seemantini K. Nadkarni[a,*]
[a]Massachusetts General Hospital, Wellman Center for Photomedicine, Harvard Medical School, Boston, Massachusetts 02114
[b]Massachusetts General Hospital, Cardiovascular Research Center and Cardiology Division, Boston, Massachusetts 02114

Abstract. Laser speckle imaging (LSI) is a novel technique for measuring the mechanical properties of atherosclerotic plaques. In LSI, the decorrelation time constant of speckle intensity fluctuations provides an index of viscoelasticity that is closely related to plaque microstructure and composition. Here, we demonstrate for the first time, the feasibility of conducting LSI *in vivo* using a prototype 1.5 mm (4.5 Fr) diameter intravascular catheter. Investigation of the catheter performance using human arterial samples *ex vivo* shows that plaque time constants measured by the LSI catheter correlate well with those measured using a free-space bulk optics system. To demonstrate LSI *in vivo*, the catheter is interfaced with a portable console for intravascular evaluation in the aorta of a living rabbit. Distinct differences in arterial time constants are identified at normal aortic and stented sites *in vivo* with intravascular LSI. © *2011 Society of Photo-Optical Instrumentation Engineers (SPIE)*. [DOI: 10.1117/1.3533322]

Keywords: Atherosclerosis; viscoelasticity; intracoronary; catheter; laser speckle imaging.

Paper 10477R received Sep. 9, 2010; revised manuscript received Dec. 9, 2010; accepted for publication Dec. 9, 2010; published online Feb. 10, 2011.

1 Introduction

Acute myocardial infarction (AMI), the leading cause of death worldwide, is frequently caused by the rupture of unstable coronary plaques.[1–5] The typical microstructural hallmarks of unstable plaques include the presence of a thin fibrous cap, a large necrotic core, and activated macrophages near the fibrous cap.[6–9] In addition to these morphological and compositional features, the mechanical properties of atherosclerotic plaques play a vital role in plaque rupture.[5,10,11] Prior studies have shown that the stress and strain distributions on the fibrous cap are modulated both by plaque microstructure and the viscoelastic properties of the atheroma, and that fibrous cap rupture primarily occurs in high stress regions.[11–13] Higher strains measured in lipid-rich tissue of low viscosity[14] are correlated with a greater propensity for plaque rupture. Histology studies have shown the localization of metalloproteinases in regions of high strain in low viscosity regions within plaques.[5] Altered viscoelastic properties of the atheroma and local hemodynamics further influence SMC and endothelial cell (EC) function.[15] Thus, there is a great deal of supporting evidence that relates plaque mechanical properties with the risk of rupture, which further enforces the need for new technologies for the mechanical evaluation of atherosclerotic plaques *in vivo*.

Laser Speckle Imaging (LSI) is a novel technique that provides information on plaque mechanical properties by measuring an index of plaque viscoelasticity.[16–18] In LSI, a coherent laser source illuminates the tissue, time-varying laser speckle patterns are acquired using a CCD or CMOS detector, and the time constant (τ) of speckle intensity decorrelation is calculated. Our prior studies, conducted *ex vivo*, have demonstrated that the speckle decorrelation time constant, τ, provides an index of plaque viscoelasticity that is closely related to key features associated with plaque stability such as fibrous cap thickness, the presence of calcific nodules, and plaque collagen and lipid contents.[16] By employing beam scanning, the spatial distribution of plaque viscoelasticity can be extracted to potentially detect focal rupture sites.[16] Spatio-temporal speckle post-processing has been previously demonstrated to enable depth-dependent speckle analysis and facilitate the measurement of fibrous cap thickness, an important parameter related with plaque stability.[17] Given its unique ability to provide both mechanical and morphological information, we anticipate that LSI will provide a powerful tool for detecting unstable plaques in patients.

In order to conduct LSI *in vivo*, a flexible, small diameter optical catheter which can safely maneuver through the coronary tree and accurately transfer speckle patterns from the coronary wall to the CMOS detector in the presence of cardiac and respiratory motion is required. Prior studies conducted on human arteries *ex vivo* have demonstrated that by using leached optical fiber bundles laser speckle patterns can be reliably transferred during motion, opening the opportunity to conduct LSI *in vivo*. However, to date the capability of LSI for mechanical evaluation of arteries has not been demonstrated *in vivo*. In this paper, we illustrate the development and validation of a new prototype intravascular LSI (ILSI) catheter for *in vivo* use and present the first demonstration of ILSI in the arteries of a living rabbit.

2 Methods

2.1 *Catheter Design*

The prototype ILSI catheter (dia. = 1.5 mm ~4.5 F) incorporates an inner optical core enclosed within a custom-fabricated

Address all correspondence to: Seemantini Nadkarni, Massachusetts General Hospital, Wellman Center of Photomedicine, Harvard Medical School, Massachusetts General Hospital - BAR 718, Boston, MA 02114; Tel.: 617-724-1381, Fax: 617 726-4103; E-mail: seemantini_nadkarni@hms.harvard.edu.

1083-3668/2011/16(2)/026005/7/$25.00 © 2011 SPIE

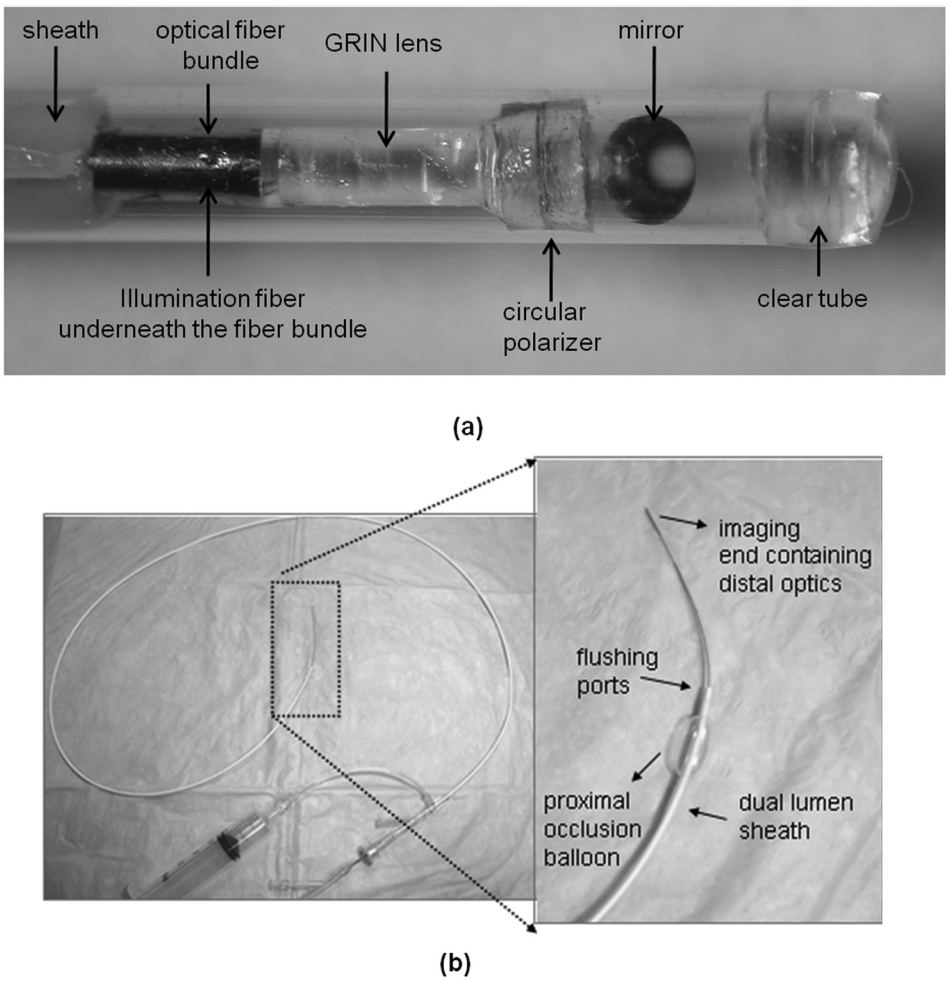

Fig. 1 *First generation prototype ILSI catheter:* (a) Distal optical assembly. The reflection of the optical fiber bundle is visible in the mirror, and the illumination fiber runs parallel is beneath the optical assembly (not visible). Scale bars: 1 mm, and (b) Custom-fabricated double lumen ILSI catheter sheath.

external sheath to facilitate intravascular delivery [Fig. 1(a)]. The optical core consists of a separate single mode optical fiber (SM 600) for arterial wall illumination which runs parallel with a leached optical fiber bundle (SCHOTT USA Inc; 4.5 k fibers, dia. = 0.7 mm) used for collecting speckle patterns from the arterial wall. The isolation of fiber elements in leached fiber bundles minimizes inter-fiber cross-talk, enabling reliable transmission of speckle patterns from the arterial wall to the camera, while providing high tolerance to bundle motion.[18] The optical assembly at the distal tip of the catheter consists of a GRIN lens (dia. = 0.7 mm, length = 1.98 mm.; NSG America Inc, New Jersy), a custom-manufactured circular polarizer disk (dia. = 1 mm) to reduce specular reflections and a 45° rod mirror to allow oblique viewing of the arterial wall. Design of the distal optical assembly is optimized for a 500 μm field of view (FOV) using ZEMAX (ZEMAX Development Corporation). To fabricate the catheter, the distal optical elements are attached in an end-to-end manner at the distal face of the fiber bundle and the terminated illumination fiber, and inserted into an optically clear protective polyethylene tube (dia. = 1.5 mm).

The custom-designed, double-lumen catheter sheath houses the optical core [Fig. 1(b)]. The inner lumen of the sheath incorporates two ports to accommodate the leached fiber bundle and the illumination fiber. The outer lumen includes a proximal occlusion balloon and flushing ports which facilitates the clearance of blood from imaging FOV, a technique commonly deployed in intracoronary Optical Coherence Tomography (OCT) and angioscopy procedures.[19,20] Also embedded in the sheath is a radio-opaque marker for visualization during fluoroscopic guidance and a distal port for rapid exchange of a standard guidewire (dia. = 360 μm).

2.2 *Portable LSI Console*

During imaging, the ILSI catheter was interfaced with a portable console [Fig. 2(a)] incorporating a Helium-Neon (He-Ne) laser (632 nm, 20 mW), an optical setup to couple light into the catheter, a high frame rate triggerable CMOS camera (Mikrotron 1310, 1280×1024 Pixel, @500 fps, ~59 dB dynamic range) for acquiring speckle patterns delivered by the fiber bundle, and a rack mounted computer equipped with a frame grabber (NI PCIe-1429) and data acquisition card (NI USB 6251 DAQ). Light from the Helium Neon laser was coupled into the single mode illumination fiber incorporated in the catheter. At a distance of 2 mm from the catheter, the beam illumination from the single mode fiber had a Gaussian profile of 160 μm. The

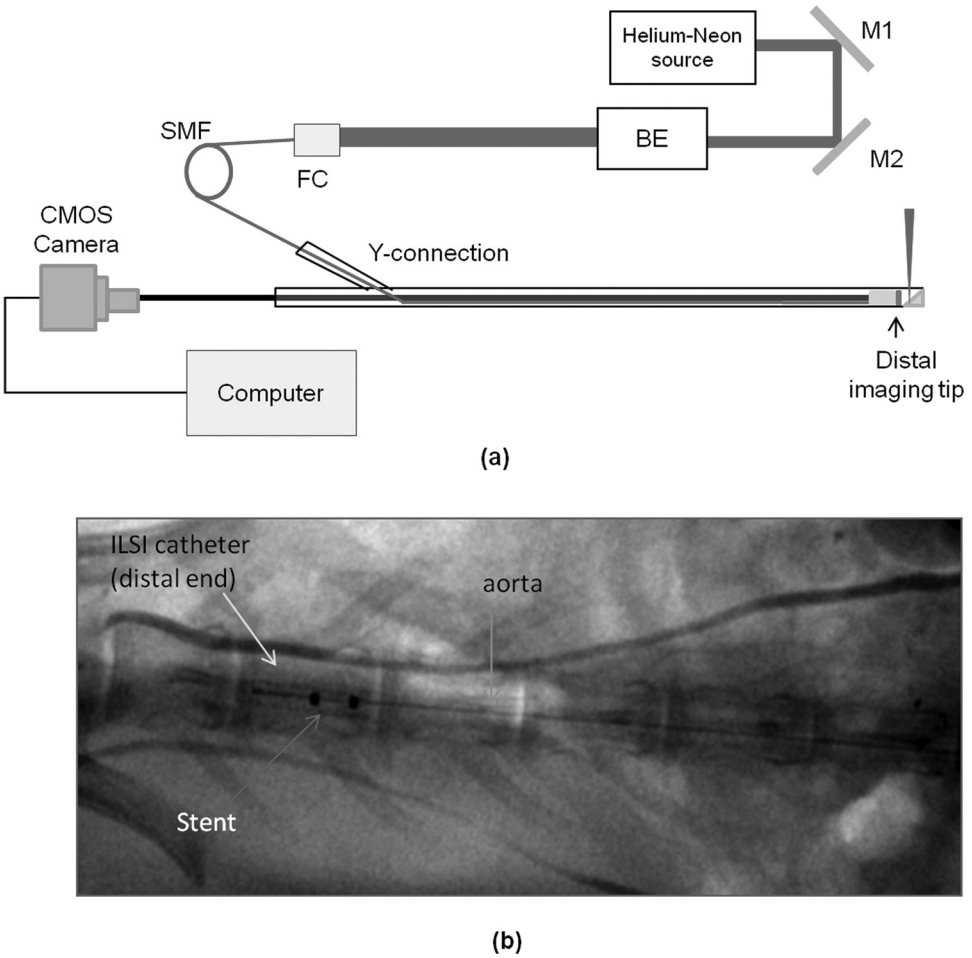

Fig. 2 (a) Schematic of ILSI system. This system incorporates a Helium-Neon light source, an optical setup to couple the laser into the catheter and a high frame-rate camera, BE: beam expander, FC: fiber coupler, M: mirror, SMF: single mode fiber. (b) Fluoroscopic snapshot of the rabbit aorta showing the embedded stent and the ILSI catheter. Two radio-opaque marks are seen on the distal end of the ILSI catheter.

light power at the sample site was 2 mW. Laser speckle patterns from the tissue were imaged on the face of the fiber bundle and transmitted to a CMOS detector via an objective lens. In order to evaluate the influence of cardiac motion on ILSI measurements, a cardiac gating module was incorporated to continuously acquire the amplified EKG and intraluminal pressure signals. During image acquisition, the cardiac gating module prospectively triggered the acquisition of first laser speckle image in synchrony with the R-wave of the EKG, followed by asynchronous acquisition of the remainder of the time varying speckle image series.

2.3 *Ex-vivo ILSI Studies*

In order to evaluate the diagnostic efficacy of the prototype ILSI catheter, τ values of human aortic plaques measured *ex vivo* using the catheter-based configuration (above), were compared with those measured using a free-space bulk optics LSI configuration, validated in our previous studies.[16,17] Briefly, in the free-space setup, light from the polarized He-Ne laser was expanded by 5:1, reflected off a mirror, and focused to a 100 μm spot on the luminal surface of the plaque and cross-polarized laser speckle images were acquired using a CMOS camera (PixeLINK PL-B761F, PixeLINK, Ottawa, ON Canada).[16,17]

Human aortic specimens ($N = 14$) were obtained from an autopsy from three patients. Immediately after harvest, the aortas were stored in phosphate buffer saline (PBS) at 4 °C and the imaging was performed at 37 °C within a PBS bath. Time varying laser speckle patterns were acquired for a duration of 4 seconds at co-registered plaque sites (marked by India ink spots) over a 500 μm FOV using both the ILSI catheter and free-space configurations. The CMOS camera integration time was set to 4 ms (frame rate of 250 frame/s) in both configurations. Speckle intensity decorrelation curves, $g_2(t)$, were measured at each plaque site using both spatial (spatial averaging window of 256×256 pixels) and temporal averaging over the time-varying image series (4 s temporal averaging window). Plaque τ values were calculated by exponential fitting of the $g_2(t)$ curves, as previously described.[16] Following imaging, plaques were fixed in 10% formalin, embedded, and sectioned for histological processing. Plaque time constants obtained from both configurations were compared by linear regression analysis and z-tests.

2.4 *In-vivo ILSI Studies*

To investigate feasibility for *in vivo* use, the prototype ILSI catheter was tested to evaluate arterial time constants in a living rabbit. To prepare for the procedure, a New Zealand

white, male rabbit was anesthetized with an IM injection of Telazol (Tiletamine HCl and Zolazepam HCl, 4.4 mg/kg, Fort Dodge Animal Health, Fort Dodge, Iowa) and intubated with an 8.0 mm endotracheal tube. Anesthesia was maintained with inhalation of isofluorane (1–4%) with supplemental oxygen. For EKG recording, a grounding pad was placed on the animal's abdomen and EKG leads were placed on all limbs, neck, and chest. The leads were interfaced into a defibrillator (Hewlett Packard CodeMasterXL+, Andover, Massachusetts) that recorded and displayed the EKG signal, and provided a digital output that fed to the cardiac gating module on the LSI console. The intra-arterial pressure signal was obtained using a pressure wire placed in the iliac artery. The EKG and pressure signals were acquired at a sampling rate of 1 kHz in conjunction with the ILSI image acquisition described below.

In order to evaluate the feasibility of ILSI in detecting differences in arterial stiffness, a coronary bare metal stent (dia. = 4 mm, length = 32 mm, VeriFlex^{TM}, Boston Scientific) was delivered and implanted in the abdominal aorta of the anesthetized rabbit under x-ray fluoroscopic guidance. The presence of the bare metal stent struts within the imaging FOV, provided focal sites of increased stiffness compared to the non-stented arterial wall. To conduct the ILSI procedure, a guide catheter (7 Fr) was inserted in the left carotid artery using a cut down approach. The ILSI catheter was introduced via the guide catheter and manually advanced into the abdominal aorta under fluoroscopic guidance. Figure 2(b) shows a fluoroscopic snapshot of the embedded stent and the ILSI catheter in the aorta of the living rabbit. Prior to imaging, the proximal occlusion balloon [Fig. 1(b)] was engaged in conjunction with continuous saline flushing to ensure that blood did not re-enter the FOV.

Laser speckle patterns were acquired over a region of interest of 288×288 pixels, at multiple discrete sites proximal to the stent at normal nonstented arterial sites, and at sites within the region of the stent. CMOS camera integration time was set to 2 ms at frame rate of 500 frames per second. To evaluate the influence of cardiac motion on ILSI measurements, acquisition of the first speckle image was triggered by the EKG, followed by asynchronous acquisition of subsequent time-varying frames over ~8 cardiac cycles (~2 s). To determine the influence of cardiac and arterial motion on ILSI measurements *in vivo*, $g_2(t)$ curves and the corresponding τ values were evaluated at cardiac phases defined by a sliding window of ~ 80 ms duration, shifted by increments of 2 ms over the cardiac cycle for imaging duration of 2 s. Following *in vivo* imaging, the rabbit was sacrificed, the abdominal aorta excised, and ILSI was conducted to evaluate arterial τ values at stented and nonstented aortic sites *ex vivo*.

3 Results

3.1 *Ex vivo Studies*

Figure 3(a) shows the normalized speckle decorrelation curves, $g_2(t)$, at three discrete human arterial sites measured *ex vivo*: fibro-calcific plaque, normal artery, and lipid plaque measured at the same location using both the catheter-based and free-space configurations. At various plaque sites in the figure, a close correspondence is noticed between the $g_2(t)$ curves measured using the catheter-based and free-space configurations. As anticipated, the lipid plaque exhibits a faster decay of the $g_2(t)$ curve due to the low viscosity of lipid compared to the normal

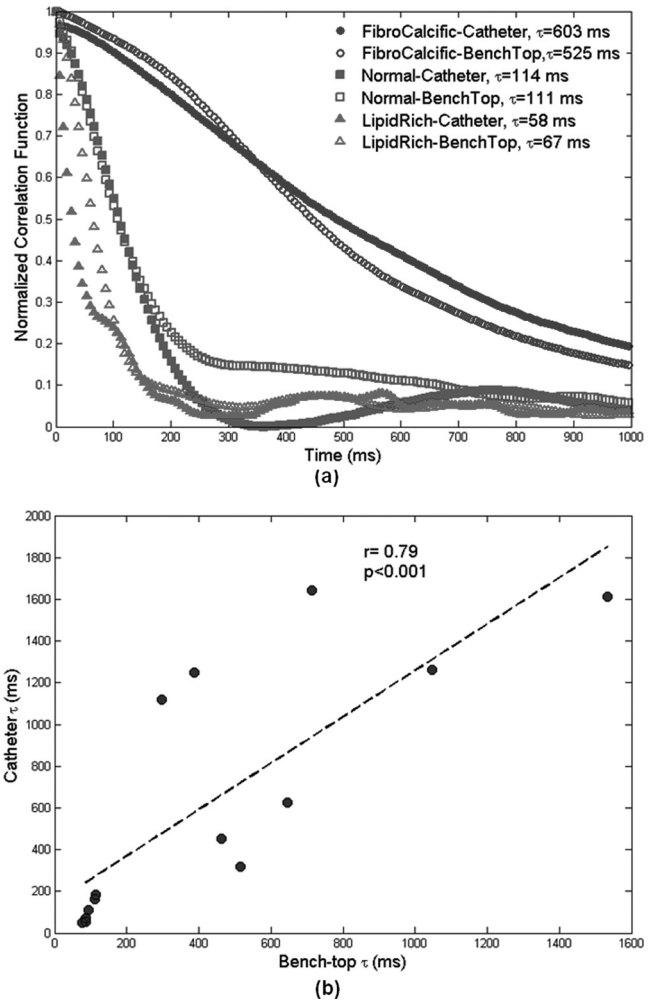

Fig. 3 *Ex vivo human arterial specimens:* (a) Speckle decorrelation curves of 3 aortic samples: fibro-calcific, normal, and lipid rich, obtained using both the catheter and bench-top systems. (b) Correlation between ILSI catheter and bench-top time constant, τ, measurements. Good correlation ($r = 0.79$, $p < 0.001$) is observed between measurements obtained using the two configurations.

and stiffer fibro-calcific lesions using both configurations. In all plaques ($N = 14$), a high correlation was observed between τ measurements obtained using the catheter-based and free-space configurations as illustrated in Fig. 3(b) ($r = 0.79$, $p < 0.001$). Furthermore, results of a z-test analysis indicated that differences in plaque τ values measured using the two configurations were not statistically significant ($p = 0.07$).

3.2 *In vivo studies*

Figure 4 shows the results of the *in vivo* ILSI study conducted in the aorta of a living rabbit. Arterial τ values (solid blue) measured *in vivo* at a stented aortic site [Fig. 4(a)] and a normal non-stented proximal site [Fig. 4(b)] are plotted at different cardiac phases over ~4 cardiac cycles. The corresponding EKG (dashed red) and pressure (dot-dashed green) signals are also shown in the figures. The average duration of the cardiac cycle was 250 ms. At the speckle pattern acquisition rate of 500 fps used in this study, arterial τ values were modulated by cardiac motion and arterial pulsation. As presented in the plots, τ varied with the cardiac cycle at both arterial sites: the coefficient

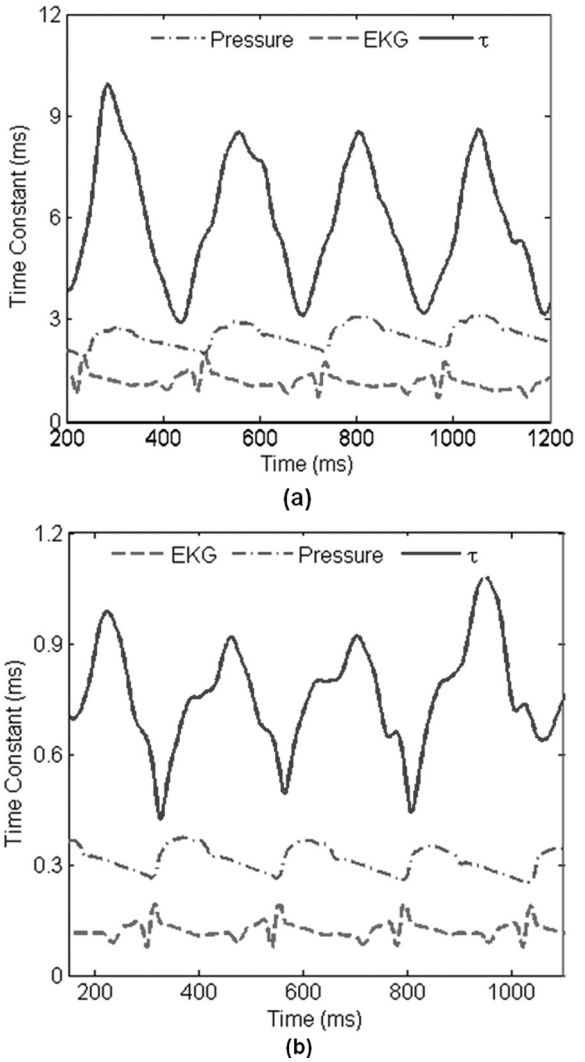

Fig. 4 *In vivo rabbit studies:* Time constant fluctuations (solid blue) at (a) an in-stent position, and (b) out of stent position, over ∼4 cardiac cycles. Corresponding EKG (dashed red) and pressure (dot-dashed green) signals are also shown. Time constants measured at the stented sites are an order of magnitude higher than those measured at nonstented proximal sites due to the presence of the bare metal stent struts in the FOV at the stented arterial sites.

of variation (COV = standard deviation/average τ) in τ over the cardiac cycle was ∼31% in the stented and ∼20% in the nonstented normal aortic sites. Time constant varied in-phase with pressure signal at the stented site [Fig. 4(a)] and peaks of τ curve coincided with peaks of pressure signal at arterial systole when arterial distention was maximized. At the nonstented normal arterial site, a time delay (∼80 ms) was observed between τ curve and the intra-arterial pressure curve [Fig. 4(b)], likely caused by the viscous phase delay of the arterial response. The mean maximum time constant measured over 4 cardiac cycles was equal to $\bar{\tau}_{\text{stent}} = 8.56 \pm 0.08$ ms at the stented site, and $\bar{\tau}_{prox} = 0.94 \pm 0.08$ ms at nonstented normal aortic site. These results indicated that distinct differences in arterial stiffness, given by statistically significant differences in τ values ($p < 0.0001$), were measured by ILSI *in vivo* in the living rabbit. The arterial τ values obtained *in vivo* at the stented and nonstented sites using ILSI were compared with those measured *ex vivo* following sacrifice. *Ex vivo* τ values ($\tau_{\text{stent}}^{exvivo} = 1.34s$, $\tau_{\text{prox}}^{exvivo} = 0.48$ s) additionally confirmed arterial stiffening occurred at stented sites relative to the normal nonstented rabbit aorta. For the first time, these results confirmed that ILSI can be reliably conducted to evaluate arterial mechanical properties *in vivo.*

4 Discussion

The process of atherosclerosis progression leading to rupture involves the complex liaison between multiple microstructural, compositional, and mechanical factors. Imaging approaches such as OCT/OFDI,[19,21] and intravascular ultrasound[22] provide vital information related to plaque microstructure and composition. Recently, photo-acoustic imaging[23] and near infrared-spectroscopy[24] have been investigated to measure lipid composition, an important factor in predicting plaque vulnerability. Raman spectroscopy[25] and near infrared fluorescence[26] approaches provide key information on biochemical and inflammatory signatures in atherosclerotic plaques. While these approaches are invaluable in evaluating key microstructural and compositional risk factors, the measurement of plaque mechanical properties provides additional fundamental information to better identify high risk coronary plaques. The ILSI approach we have developed provides the unique capability of measuring an index of plaque viscoelasticity that is potentially intimately related with the propensity of plaque rupture. We anticipate that someday, ILSI can be conducted as a stand-alone approach or can provide a powerful adjunct to complement other intravascular imaging approaches that measure plaque microstructure and composition.

In the current study, we described the fabrication, validation, and first *in vivo* demonstration of a new ILSI catheter-based system. This system includes a prototype ILSI catheter incorporated for use with a portable console. The size of the first generation prototype catheter used in this study is 4.5 F (∼1.5 mm). This catheter is equipped with a proximal occlusion balloon and flushing ports to clear blood from the FOV during imaging. Our future catheter designs will focus on significantly reducing catheter size (∼0.8–1 mm) by incorporating smaller diameter custom-fabricated fiber bundles that can be safely guided into patient coronary arteries. The ILSI catheter performance was validated using both *ex vivo* studies on human arterial samples and *in vivo* rabbit studies.

The *ex vivo* studies demonstrated an adequate correlation between the catheter-based ILSI measurements with those obtained using a free-space bulk optics set up, which verified the equivalence of the two configurations (Fig. 3). Potential discrepancies in plaque τ values were likely caused by offsets in the exact imaging site and co-registration errors when each sample site was measured using the two configurations.

In the aorta of a living rabbit, our results demonstrated that ILSI can differentiate regional arterial stiffness *in vivo* under physiological conditions of arterial motion (Fig. 4). ILSI τ values measured at discrete sites within the stent, exhibited a statistically significant ∼10-fold increase compared to τ values measured at normal regions proximal to the stent. These results were compatible with our expectations that the presence of bare metal stent struts within the FOV causes considerable stiffening of the arterial wall compared to normal nonstented

aortic sites. ILSI measurements of the excised aorta following sacrifice additionally confirmed that arterial stiffening occurred due to stent placement, as evidenced by the significantly higher time constants measured at the stented versus nonstented sites *ex vivo*.

Our results [Fig. 4(a) and 4(b)] revealed that arterial time constants are modulated by the intra-arterial pressure waveform. The cardiac phase dependent variation in τ also likely provides information about the strain induced in the arterial wall in response to the cyclic intra-luminal pressure. The in-phase variation of τ with the pressure signal at the stented site[27] was likely evoked by the presence of linearly elastic stent struts,[28] which strained in phase with the intraluminal pressure wave. On the other hand, at the nonstented normal arterial site, the τ curve lagged the pressure signal with peak τ occurring $\sim$80 ms after peak systole, which may be attributed to hysteresis loss due to the viscoelastic properties of the normal arterial wall.[28] This information also resulted in larger coefficient of variation in the stented site compared to normal artery, potentially implying viscous dissipation in the normal nonstented region.

Temporal resolution in measuring τ variations over the cardiac cycle is determined by the size of the sliding window. A shorter window could enhance the temporal resolution and enable observation of finer details of τ variation. However, during post-processing, temporal (circular) averaging over multiple $g_2(t)$ curves is needed to provide statistical averaging. Given this exchange between temporal resolution and need for sufficient averaging, in the current study, we chose the sliding window size of 80 ms matched to be the same average duration as of diastolic phase and circular averaging was performed over 40 temporally evolving $g_2(t)$ curves. While the opportunity to conduct ILSI *in vivo* to measure an index of arterial viscoelasticity is promising, in the current study, the τ variation over the cardiac cycle measured using a CMOS acquisition rate of 500 fps, warrants the cardiac gated approach adapted at this juncture. This adds significant time to the imaging procedure, limiting the evaluation to only discrete arterial lesions. Instead, a nongated approach will facilitate rapid imaging of long arterial segments potentially enabling the use of ILSI device as a screening tool to identify high-risk plaques in patients. Given the low frequency of cardiac motion relative to the high rate of speckle decorrelation ($<$20 ms *in vivo*), we anticipate that sufficient motion stability can be achieved to conduct nongated ILSI in future studies, by employing high speed CMOS detectors capable of higher image acquisition rates ($>$1 kHz) to measure laser speckle fluctuations over very short time scales. In the current study, due to considerably lower frequency of respiratory motion ($\sim$1Hz) compared to the CMOS acquisition rate, its effects were negligible and respiratory gating was not required.

In addition to cardiac and respiratory motion, blood flow is another major impediment for intravascular optical imaging procedures. In the current *in vivo* procedure, balloon occlusion was employed in conjunction with a continuous saline flushing to displace blood. When the balloon was fully engaged, sufficient resistance to the saline flush was perceived which ensured that blood was removed from the FOV. Confirmation of blood clearance was completed using fluoroscopic visualization by replacing the saline flush with a radio opaque contrast solution which indicated that no blood was present distal to the balloon within the imaging FOV. Similarly, prior studies using intracoronary OCT *in vivo* have demonstrated that saline flushing sufficiently clears the arterial lumen and no scattering signal from residual RBCs is detected during saline purging.[21] Given the observations of these studies indicating that sufficient blood clearance can be obtained during saline flushing and the inclusion of proximal balloon occlusion in our current study to ensure that blood did not re-enter the FOV during imaging, sufficient verification was obtained that the RBC scattering signal was negligible in the *in vivo* ILSI measurements.

In both the *ex vivo* and *in vivo* studies, we demonstrated the feasibility of the ILSI approach by conducting spatial averaging over the entire FOV ($\sim$500 μm), and depth-dependent and spatially resolved variations in τ were lost. In theory, τ can be measured from $g_2(t)$ functions over a single speckle spot. The speckle size is determined by the geometry of the illumination and collection optics and in the current catheter configuration, speckle size is matched to a single fiber strand diameter $\sim$8 μm. However, in practice, calculating intensity decorrelation time using only a single speckle spot requires sufficient temporal averaging over long imaging durations to obtain necessary statistical accuracy which is intractable in cardiovascular applications due to cardiac motion considerations.[29] Instead, spatial (ensemble) averaging over neighboring pixels can be employed to obtain sufficient speckle statistics over shorter imaging times while reducing spatial resolution. In future studies, high-resolution mapping of arterial τ distributions can be obtained by optimizing this trade-off between spatial resolution and imaging duration. We have previously revealed that by using beam scanning and spatio-temporal post-processing,[17] spatially-resolved and depth-dependent measurements of variations in time constants can be obtained. In future studies, these previous methods can be implemented in conjunction with mechanisms for rotational scanning the arterial circumference[19,21] during longitudinal pull-back to facilitate spatial and depth-dependent mapping of heterogeneities of wall viscoelasticity.

ILSI utilizes a speckle based approach which is highly sensitive to small phase shifts induced by particle displacements on the order of less than a wavelength within the illuminated volume. Therefore, ILSI potentially provides exquisite sensitivity to small variations in arterial mechanical properties. In practice, sensitivity of ILSI in detecting small variations in tissue mechanical properties is also governed by the experimental configuration including detector shot noise, CMOS camera dynamic range, and pixel digitization effects. Speckle contrast is another important parameter that affects sensitivity by setting the plateau level of $g_2(t)$ curve and is a function of parameters, such as laser coherence length (or line-width), pixel to speckle ratio, and frame rate. In this study, the long coherence length of Helium-Neon (20 cm) provided adequate speckle contrast.[30] The pixel to speckle ratio was also matched to be less than one to maximize the contrast. Moreover, sufficiently the high frame rate was employed to reduce effects of speckle blurring due to rapid speckle decorrelation observed under *in vivo* conditions.

In the current study, the stented rabbit model was used to test the feasibility of ILSI approach *in vivo*. The implanted coronary stent focally increased arterial stiffness relative to the adjacent nonstented normal arterial wall. Currently, we are conducting

further *in vivo* studies to assess the ability of ILSI approach to evaluate plaque viscoelasticity in coronary arteries using animal models of atherosclerosis. The development and *in vivo* demonstration of the ILSI prototype catheter described at this time, opens the exciting opportunity for future clinical studies to obtain invaluable insights on key mechanical metrics related to plaque rupture.

Acknowledgments

The authors thank Jose-Luiz Guerrero and Adam Mauskapf for their assistance in conducting *in vivo* animal studies. This work was supported in part by the NIH Grant Nos. R21 HL 088306 (S.N) and the ARRA R21 HL 088306-02S1 (S.N.).

Reference

1. R. T. Lee and P. Libby, "The unstable atheroma," *Arterioscler. Thromb. Vasc. Biol.* **17**, 1859–1867 (1997).
2. P. Libby, "Molecular bases of the acute coronary syndromes," *Circulation* **91**, 2844–2850 (1995).
3. E. Falk, P. K. Shah, and V. Fuster, "Coronary plaque disruption," *Circulation* **92**, 657–671 (1995).
4. J. E. Muller, G. H. Tofler, and P. H. Stone, "Circadian variation and triggers of onset of acute cardiovascular disease," *Circulation* **79**, 733–743 (1989).
5. L. H. Arroyo and R. T. Lee, "Mechanisms of plaque rupture: mechanical and biologic interactions," *Cardiovasc. Res.* **41**, 369–375 (1999).
6. R. Virmani, F. D. Kolodgie, A. P. Burke, A. Farb, and S.M. Schwartz, "Lessons from sudden coronary death: a comprehensive morphological classification scheme for atherosclerotic lesions," *Arterioscler., Thromb., Vasc. Biol.* **20**, 1262–1275 (2000).
7. A. P. Schroeder and E. Falk, "Vulnerable and dangerous coronary plaques," *Atherosclerosis* **118** Suppl, S141–149 (1995).
8. F. D. Kolodgie, A. P. Burke, A. Farb, H. K. Gold, J. Yuan, J. Narula, A. V. Finn, and R. Virmani, "The thin-cap fibroatheroma: a type of vulnerable plaque: the major precursor lesion to acute coronary syndromes," *Curr. Opin. Cardiol.* **16**, 285–292 (2001).
9. R. Virmani, A. P. Burke, F. D. Kolodgie, and A. Farb, "Vulnerable plaque: the pathology of unstable coronary lesions," *J. Interv. Cardiol.* **15**, 439–446 (2002).
10. H. M. Loree, B. J. Tobias, L. J. Gibson, R. D. Kamm, D. M. Small, and R. T. Lee, "Mechanical properties of model atherosclerotic lesion lipid pools," *Arterioscler. Thromb.* **14**, 230–234 (1994).
11. P. D. Richardson, M. J. Davies, and G. V. Born, "Influence of plaque configuration and stress distribution on fissuring of coronary atherosclerotic plaques," *Lancet* **2**, 941–944 (1989).
12. H. M. Loree, R. D. Kamm, R. G. Stringfellow, and R. T. Lee, "Effects of fibrous cap thickness on peak circumferential stress in model atherosclerotic vessels," *Circ. Res.* **71**, 850–858 (1992).
13. J. Ohayon, P. Teppaz, G. Finet, and G. Rioufol, "In-vivo prediction of human coronary plaque rupture location using intravascular ultrasound and the finite element method," *Coron. Artery Dis.* **12**, 655–663 (2001).
14. J. A. Schaar, C. L. De Korte, F. Mastik, C. Strijder, G. Pasterkamp, E. Boersma, P. W. Serruys, and A. F. Van Der Steen, "Characterizing vulnerable plaque features with intravascular elastography," *Circulation* **108**, 2636–2641 (2003).
15. D. Ingber, "Mechanical signalling and cellular response to extracellular matrix in angiogenesis and cardiovascular physiology," *Circ. Res.* **91**, 877–887 (2002).
16. S. K. Nadkarni, B. E. Bouma, T. Helg, R. Chan, E. Halpern, A. Chau, M. S. Minsky, J. T. Motz, S. L. Houser, and G. J. Tearney, "Characterization of atherosclerotic plaques by laser speckle imaging," *Circulation* **112**, 885–892 (2005).
17. S. K. Nadkarni, A. Bilenca, B. E. Bouma, and G. J. Tearney, "Measurement of fibrous cap thickness in atherosclerotic plaques by spatiotemporal analysis of laser speckle images," *J. Biomed. Opt.* **11**, 021006 (2006).
18. S. K. Nadkarni, B. E. Bouma, D. Yelin, A. Gulati, and G. J. Tearney, "Laser speckle imaging of atherosclerotic plaques through optical fiber bundles," *J. Biomed. Opt.* **13**, 054016 (2008).
19. I. K. Jang, B. E. Bouma, D. H. Kang, S. J. Park, S. W. Park, K. B. Seung, K. B. Choi, M. Shishkov, K. Schlendorf, E. Pomerantsev, S. L. Houser, H. T. Aretz, and G. J. Tearney, "Visualization of coronary atherosclerotic plaques in patients using optical coherence tomography: comparison with intravascular ultrasound," *J. Am. Coll. Cardiol.* **39**, 604–609 (2002).
20. Y. Uchida, Y. Fujimori, J. Hirose, and T. Oshima, "Percutaneous coronary angioscopy," *Jpn .Heart. J.* **33**, 271–294 (1992).
21. G. J. Tearney, S. Waxman, M. Shishkov, B. J. Vakoc, M. J. Suter, M. I. Freilich, A. E. Desjardins, W. Y. Oh, L. A. Bartlett, M. Rosenberg, and B. E. Bouma, "Three-dimensional coronary artery microscopy by intracoronary optical frequency domain imaging," *JACC Cardiovasc. Imaging* **1**, 752–761 (2008).
22. P. R. Liebson and L. W. Klein, "Intravascular ultrasound in coronary atherosclerosis: a new approach to clinical assessment," *Am. Heart. J.* **123**, 1643–1660 (1992).
23. S. Sethuraman, S. R. Aglyamov, J. H. Amirian, R. W. Smalling, and S. Y. Emelianov, "Intravascular photoacoustic imaging using an IVUS imaging catheter," *IEEE TransUltrason. Ferroelectr. Freq. Control* **54**, 978–986 (2007).
24. P. R. Moreno, R. A. Lodder, K. R. Purushothaman, W. E. Charash, W. N. O'Connor, and J. E. Muller, "Detection of lipid pool, thin fibrous cap, and inflammatory cells in human aortic atherosclerotic plaques by near-infrared spectroscopy," *Circulation* **105**, 923–927 (2002).
25. A. H. Chau, J. T. Motz, J. A. Gardecki, S. Waxman, B. E. Bouma, and G. J. Tearney, "Fingerprint and high-wavenumber Raman spectroscopy in a human-swine coronary xenograft in vivo," *J. Biomed. Opt.* **13**, 040501 (2008).
26. M. A. Calfon, C. Vinegoni, V. Ntziachristos, and F. A. Jaffer, "Intravascular near-infrared fluorescence molecular imaging of atherosclerosis: toward coronary arterial visualization of biologically high-risk plaques," *J. Biomed. Opt.* **15**, 011107.
27. P. H. Rolland, A. B. Charifi, C. Verrier, H. Bodard, A. Friggi, P. Piquet, G. Moulin, and J. M. Bartoli, "Hemodynamics and wall mechanics after stent placement in swine iliac arteries: comparative results from six stent designs," *Radiology* **213**, 229–246 (1999).
28. S. Canic, K. Ravi-Chandar, Z. Krajcer, D. Mirkovic, and S. Lapin, "Mathematical Model analysis of Wallstent and Aneurx: dynamic responses of bare-metal endoprosthesis compared with those of stent-graft," *Tex. Heart Inst. J.* **32**, 502–506 (2005).
29. L. Cipelletti and D. A. Weitz, "Ultralow angle dynamic light scattering with a charge coupled device camera based multispeckle multitau correlator," *Rev. Sci. Instr.* **70**, 3214–3221 (1999).
30. J. W. Goodman, *Speckle Phenomena in Optics: Theory and Applications*, Roberts & Co., Englewood, CO (2007).